WARSAW UNIVERSITY OF TECHNOLOGY Index 351733
FACULTY OF CIVIL ENGINEERING
COMMITTEE FOR CIVIL AND WATER ENGINEERING
POLISH ACADEMY OF SCIENCES ISSN 1230-2945

DOI: 10.24425/ace.2023.147652

ARCHIVES OF CIVIL ENGINEERING

Vol. LXIX ISSUE 4 2023

pp. 141 –156

Research paper

Influence of soil anisotropic stiffness on the deformation induced by an open pit excavation

Katarzyna Lisewska[1], Marcin Cudny[2]

Abstract: In this paper, the problem of deformation induced by an open pit excavation in anisotropic stiff soils is analysed by FE modelling. The presented research is focused on the influence of material model with anisotropic stiffness on the accuracy of deformation predictions as compared with the field measurements. A new hyperelastic-plastic model is applied to simulate anisotropic mechanical behaviour of stiff soils. It is capable to reproduce mixed variable stress-induced anisotropy and constant inherent cross-anisotropy of the small strain stiffness. The degradation of stiffness depending on strain is modelled with the Brick-type model. The model formulation and parameters are briefly presented. General deformation pattern obtained in the exemplary 2D boundary value problem of an open pit excavation is investigated considering different values of inherent cross-anisotropy coefficient of small strain stiffness. The numerical simulations are performed as a coupled deformation-flow analysis which allows to properly model the drainage conditions. The excavation phases are simulated by removal of soil layers according to the realistic time schedule. Finally, the monitored case of the trial open pit excavation in heavily overconsolidated Oxford Clay at Elstow, UK is simulated with proposed material model both in 2D and 3D conditions. The obtained calculation results are compared with displacement measurements and discussed.

Keywords: soil stiffness anisotropy, stiff overconsolidated clays, open pit excavation, FE modelling

[1]MSc., Eng., Gdańsk University of Technology, Faculty of Civil and Environmental Engineering, ul. Gabriela Narutowicza 11/12, 80-233 Gdańsk, Poland, e-mail: katkowa3@pg.edu.pl, ORCID: 0000-0002-5184-9747
[2]DSc., PhD., Eng., Gdańsk University of Technology, Faculty of Civil and Environmental Engineering, ul. Gabriela Narutowicza 11/12, 80-233 Gdańsk, Poland, e-mail: mcud@pg.edu.pl, ORCID: 0000-0003-3446-1940

1. Introduction

Numerical modelling of geotechnical problems related to the subsoil unloading (e.g. tunneling, excavations) requires an appropriate material description of the soil behaviour, which allows possibly accurate simulation of the mechanical characteristics in the range of small strains [1, 2]. The most important elements here are the pre-failure stiffness non-linearity related to the barotropy and strain degradation of the current stiffness moduli as well as stiffness anisotropy. Constitutive models available in popular computational systems rarely allow to take into account the stiffness anisotropy in the range of small deformations. Most frequently, it results from a more complicated formulation and implementation than in the case of isotropic models. The limited availability of additional material parameters associated with anisotropy is another reason. However, the development of measurement techniques in experimental soil mechanics, observed in recent years, allows to design and conduct precise investigations of the stiffness anisotropy [3]. In the laboratory, most often it is the measurement of cross-anisotropic shear moduli in the triaxial apparatus equipped with the seismic bender elements oriented both vertically and horizontally. Verification of the formulated anisotropic models is possible in element tests, nevertheless, the most challenging is the final application of the developed model in the real boundary value problem (BVP). Due to the complexity related not only to the material description but also to the modelling of drainage conditions, groundwater flow, consolidation and heterogeneous geological structure, the robustness and simplicity of the constitutive model are very important. Numerical simulations of geotechnical BVPs may concern parametric studies of exemplary problems but it is very valuable to perform simulations of real case studies and compare their results with the field measurements. In this paper, a unique case study of the instrumented trial open excavation pit in Oxford Clay, at Elstow, the UK [4, 5] is analysed. The main aim of this trial excavation was not to focus on the standard slope stability problem, as the soil is highly overconsolidated and very stiff exhibiting a high shear strength properties, but to deliver deformation measurements which can be used in a real scale verification of new soil models. Since the Oxford Clay displays a high degree of the inherent stiffness anisotropy, it was an opportunity to perform back analysis of the excavation with the recently developed anisotropic hyperelastic-plastic model for stiff anisotropic soils [6, 7]. The model is briefly introduced before being used in the FE simulations of the exemplary open pit excavation problem and subsequently in the back analysis of the trial excavation in Oxford Clay.

2. Anisotropic hyperelastic-plastic model for stiff soils

The preliminary version of the used constitutive model was formulated and verified in selected element tests with available experimental evidence in [6, 7]. The model was also applied in FE analyses of BVPs of tunneling and supported excavation [6, 9]. The model is based on the small strain anisotropic hyperelastic kernel subjected to the strain degradation of the reference tangent shear modulus within the stress limits of conventional

isotropic shear strength criterion in the stress space. It is implemented into the *Plaxis* FE code [10] via User Defined Soil Model (UDSM) facility. The main elements of the model are concisely described in the following subsections.

2.1. Small strain anisotropic hyperelastic kernel

The detailed description of the applied hyperelastic model used in the small strain kernel is published in [7]. It is a modification of Vermeer's hyperelastic model [11] by incorporation of the inherent cross-anisotropy. In the original Vermeer's formulation the elastic potential is a function of the effective stress σ which provides the stress-induced anisotropy of the resulting hyperelastic stiffness. In the modified formulation, the inherent anisotropy is incorporated by the joint stress–microstructure invariant Q_M defined as:

$$Q_M(\boldsymbol{\sigma}, \mathbf{M}) = \frac{1}{2}\mathrm{tr}\left(\boldsymbol{\sigma}^2 \cdot \mathbf{M}\right) = \frac{1}{2} M_{ij}\sigma_{jk}\sigma_{ki} \tag{2.1}$$

where $\mathbf{M}$ is the second-order tensor defining an anisotropic microstructure [12]. In the case of cross-anisotropy, its components are calculated from the following dyadic product:

$$\mathbf{M} = \mathbf{v} \otimes \mathbf{v}, \qquad M_{ij} = v_i v_j \tag{2.2}$$

where the unit vector $\mathbf{v}$ identifies the symmetry axis normal to the plane of isotropy in the cross-anisotropic material. The horizontally oriented plane of isotropy is examined in this paper. The symmetry axis is vertical, i.e. $\mathbf{v} = [0, 1, 0]^T$, which leads to $\mathbf{M} = \mathrm{diag}(0, 1, 0)$. As a measure of the degree of inherent cross-anisotropy the coefficient α_G [13, 14] is used:

$$\alpha_G = \frac{G_{0hh}}{G_{0vh}} \tag{2.3}$$

where, G_{0vh} is the small strain shear modulus in the vertical plane and G_{0hh} is the small strain shear modulus in the horizontal plane of isotropy. It should be noted that shear moduli G_{0vh} and G_{0hh} need to be determined under the isotropic stress state $\boldsymbol{\sigma} = \mathrm{diag}(p_0, p_0, p_0)$ in order to express the pure inherent cross-anisotropy by the coefficient α_G. In the formulation of the modified anisotropic hyperelastic model the following mixed invariant is applied which groups both stress and joint stress-microstructure invariants:

$$\overline{Q}(\boldsymbol{\sigma}, \mathbf{M}) = \frac{1}{2}\overbrace{\left[\sigma_{ij} + 2(\alpha_G - 1)M_{ij}\right]}^{m_{ij}}\sigma_{jk}\sigma_{ki} = \frac{1}{2} m_{ij}\sigma_{jk}\sigma_{ki} \tag{2.4}$$

where, δ_{ij} is the Kronecker symbol. The anisotropic elastic potential in the modified formulation is defined as:

$$\overline{W}(\boldsymbol{\sigma}, \mathbf{M}) = \frac{\left(p_{\mathrm{ref}}\sqrt{\frac{1}{2} + \alpha_G}\right)^{1-\beta}}{\alpha_G G_{0vh}^{\mathrm{ref}}(1+\beta)}\overline{Q}(\boldsymbol{\sigma}, \mathbf{M})^{\frac{(1+\beta)}{2}} \tag{2.5}$$

where G_{0vh}^{ref} is the reference shear modulus in vertical plane measured at the reference isotropic stress $p_0 = p_{\mathrm{ref}}$ and β is a material parameter coupling the order of stiffness stress dependency and the Poisson's ratio. The second stress derivative of the elastic potential gives the tangent compliance tensor $\mathbf{C}^t(\sigma, \mathbf{M})$ of the anisotropic hyperelastic model:

$$C_{ijkl}^{\mathrm{t}} = \frac{\partial^2 \overline{W}(\boldsymbol{\sigma}, \mathbf{M})}{\partial \sigma_{ij} \partial \sigma_{kl}} = \frac{\left(p_{\mathrm{ref}} \sqrt{\frac{1}{2} + \alpha_G} \right)^{1-\beta}}{4 \alpha_G G_{0vh}^{\mathrm{ref}}} \overline{Q}^{\frac{(\beta-1)}{2}} A_{ijkl} \tag{2.6}$$

where

$$A_{ijkl} = \left(\delta_{jl} m_{ik} + \delta_{il} m_{jk} \right)^{\mathrm{symm}} - (1-\beta) \frac{\left(\sigma_{al} m_{ak} + \sigma_{bk} m_{bl} \right) \left(\sigma_{aj} m_{ai} + \sigma_{bi} m_{bj} \right)}{4 \overline{Q}(\boldsymbol{\sigma}, \mathbf{M})} \tag{2.7}$$

and

$$\left(\delta_{jl} m_{ik} + \delta_{il} m_{jk} \right)^{\mathrm{symm}} = \frac{1}{2} \left(\delta_{jl} m_{ik} + \delta_{jk} m_{il} + \delta_{il} m_{jk} + \delta_{ik} m_{jl} \right) \tag{2.8}$$

In the numerical implementation the 4-th order compliance tensor is transformed to the Voigt matrix notation and inverted analytically or numerically (a general 3D case with an arbitrary orientation of the plane of isotropy) to obtain tangent stiffness matrix.

The parameters of the anisotropic hyperelastic model are: G_{0vh}^{ref}, α_G, β, p_{ref}. The resulting stiffness is a homogeneous function of stress of order $1 - \beta$. The stress-induced component of stiffness anisotropy changes with the current stress obliquity and principal stress directions, whereas the inherent component of stiffness anisotropy is constant and cross-anisotropic with the axis of symmetry defined by the unit vector $\mathbf{v}$. In the classical linear elastic description, a cross-anisotropic stiffness requires the definition of five independent material constants [15]. In the presented model two classical shear moduli are used, i.e. G_{0vh}^{ref}, $G_{0hh}^{\mathrm{ref}} = \alpha_G G_{0vh}^{\mathrm{ref}}$. The remaining classical cross-anisotropic constants like directional Young's moduli and Poisson's ratios can be derived from the stiffness and compliance tensors. It is presented in [7].

2.2. Stiffness strain degradation

The pre-failure behaviour concerning gradual strain degradation of the stiffness is simulated with the Brick-type model based on the original formulation by Simpson [16]. The Brick model may be classified as an example of the nested yield surfaces concept defined in the strain space [17, 18]. It allows to simulate stiffness degradation during monotonic loading and regain of high initial stiffness after sharp load reversals. Different versions of the Brick-type model are reported in the literature giving satisfactory results in various FE computations, e.g. [19–21]. The Brick algorithm used in the calculations presented in this paper adheres to the implementation details published in [22].

The idea of the stiffness degradation model is presented schematically in Fig. 1. It uses the analogy of a man pulling the finite number N_{b} of bricks on strings (here $N_{\mathrm{b}} = 3$).

Initially strings of different lengths s^j are slack (Fig. 1 – (1)) and the actual tangent reference shear modulus G^{ref}_{vht} is equal to the initial value G^{ref}_{0vh}. When the man moves, the strings become taut one by one, pulling the next brick. The man's movement represents strain and the strings lengths are radii of the nested circular yield surfaces in the strain space. Every time the next brick starts being pulled by the man, the tangent shear modulus G^{ref}_{vht} is degraded in steps of height $\Delta\omega^j_G$ (Fig. 1 – (2)). When all bricks are pulled (Fig. 1 – (3)), the reference shear modulus achieves the constant minimum value $G^{\text{ref}}_{vht\,\min}$. In the analogous Brick formulation described in [22] the minimum value of the reference shear modulus is denoted as G^{ref}_{ur} and identified with the unloading-reloading stiffness. When the loading direction in the strain space changes, the strings are loosen and the high initial modulus G^{ref}_{0vh} is regained (Fig. 1 – (4)).

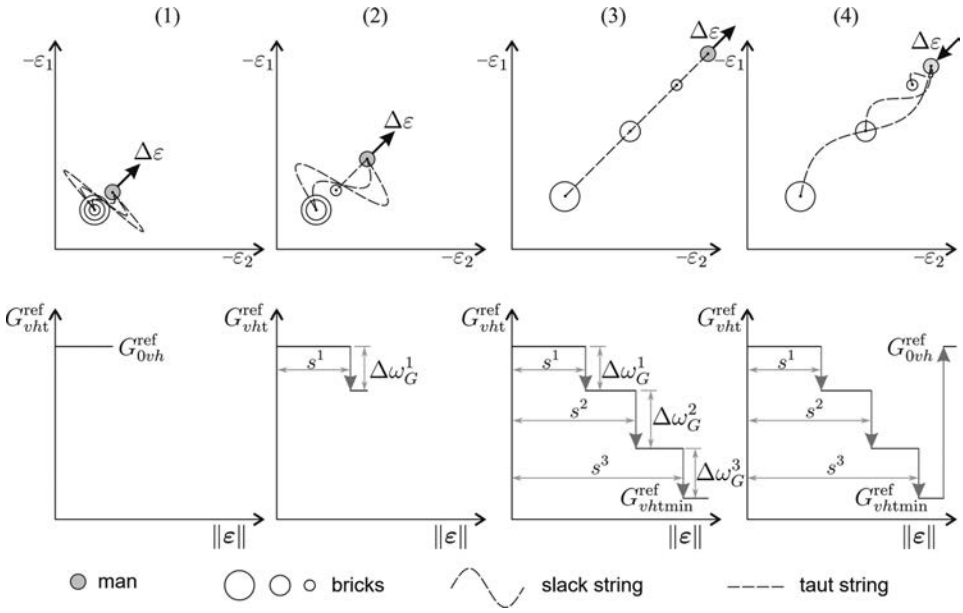

Fig. 1. Concept of the Brick-type model of stiffness strain degradation presented in the exemplary monotonic strain path (1–3) followed by sharp unloading (4)

The relative strain distances between the man and bricks are measured by the Euclidian norm of the strain $\|\boldsymbol{\varepsilon}\| = (\varepsilon_{ij}\varepsilon_{ij})^{0.5}$. Parameters concerning the applied Brick model for the pre-failure behaviour describe the stepwise representation of the *S*-shaped curve presented in Fig. 1. The S-shape curve is based on the following continuous model of the degradation of the stiffness ratio:

$$\frac{G^{\text{ref}}_{vht}}{G^{\text{ref}}_{0vh}} = \left(\frac{\|\boldsymbol{\varepsilon}\|_{\text{sh}}}{\|\boldsymbol{\varepsilon}\|_{\text{sh}} + \frac{3}{7}\|\boldsymbol{\varepsilon}\|} \right)^2 \tag{2.9}$$

where $\|\boldsymbol{\varepsilon}\|_{\mathrm{sh}}$ is the shape parameter controlling the steepness of the S-shaped curve. The stepwise model applied in the calculations employs $N_{\mathrm{b}} = 10$ bricks to trace the strain history with equal step heights called the stiffness proportions:

$$\Delta\omega_G = \frac{G^{\mathrm{ref}}_{0vh} - G^{\mathrm{ref}}_{vht}}{N_{\mathrm{b}} G^{\mathrm{ref}}_{0vh}} \tag{2.10}$$

The string lengths s^j for every j-th brick ($j = 1, \ldots, N_{\mathrm{b}}$), numbered according to the length, are calculated from:

$$s^j = \frac{7}{3}\|\boldsymbol{\varepsilon}\|_{\mathrm{sh}} \left(\sqrt{\frac{1}{1.0 - j\Delta\omega_G + 0.5\Delta\omega_G}} - 1 \right) \tag{2.11}$$

All presented simulations are performed with a displacement based FE program [10] and in the stress integration procedure the strain increment $\Delta\boldsymbol{\varepsilon}$ is known. First, the following condition is controlled for every j-th brick:

$$d^j = \left\| \boldsymbol{\varepsilon} + \Delta\boldsymbol{\varepsilon} - \boldsymbol{\varepsilon}^{\mathrm{b}j} \right\| > s^j \tag{2.12}$$

When the distance d^j exceeds the string length s^j then the j-th brick is assumed active and its location should be updated by the following strain increment:

$$\Delta\boldsymbol{\varepsilon}^{\mathrm{b}j} = \left(\boldsymbol{\varepsilon} + \Delta\boldsymbol{\varepsilon} - \boldsymbol{\varepsilon}^{\mathrm{b}j} \right) \frac{d^j - s^j}{d^j} \tag{2.13}$$

Once the number of active bricks n_{ab} is counted, the actual tangent reference modulus can be determined:

$$G^{\mathrm{ref}}_{vht} = G^{\mathrm{ref}}_{vh0}\left(1 - n_{\mathrm{ab}}\Delta\omega_G\right) \tag{2.14}$$

which is used to calculate the components of the hyperelastic stiffness matrix and consequently the stress increment $\Delta\boldsymbol{\sigma}$.

2.3. Shear strength criterion

The employed stiffness degradation model by itself cannot provide the correct control of the shear strength, i.e. the mobilised friction may exceed the value of the internal friction angle. Hence, in the proposed constitutive model the shear strength is simply controlled by the conventional stress-based isotropic Matsuoka-Nakai criterion [23]:

$$F_{\mathrm{MN}}(\boldsymbol{\sigma}) = I_1 I_2 - \frac{9 - \sin^2\phi}{-1 + \sin^2\phi} I_3 \leq 0 \tag{2.15}$$

where ϕ is the effective friction angle and I_1, I_2, I_3 are the stress invariants defined as:

$$I_1 = \sigma_{kk}, \qquad I_2 = \frac{1}{2}\left[\sigma_{ij}\sigma_{ij} - (I_1)^2\right], \qquad I_3 = \det(\boldsymbol{\sigma}) \tag{2.16}$$

The effective cohesion parameter c, is incorporated into the criterion by calculating the stress invariants in Eq. (2.16) for the stress state: $\sigma - p_c\delta$, with $p_c = c \cdot \cot\phi$. Additionally, the admissible stress states are limited by the Rankine tension cut-off criterion $p \geq p_{\text{te}}$.

In the flow rule, the Drucker–Prager function is applied as the plastic potential:

$$G_{\text{DP}}(\boldsymbol{\sigma}) = q - \frac{6\sin\psi}{3-\sin\psi}p \tag{2.17}$$

where ψ is the dilatancy angle.

When the stress state calculated in the Brick part of the model does not conform with the shear strength criterion from Eq. (2.15), it is returned to the yield surface $F_{\text{MN}} = 0$. To this end, the implicit return mapping algorithm is applied as described in [24].

3. Simple example of an open pit excavation problem

Before the presented anisotropic hyperelastic-plastic model is used in the FE back analysis of the real case, a simple exemplary BVP of an open pit excavation in plane strain conditions is examined. The main aim is to analyse the influence of the pure inherent cross-anisotropy on the deformation pattern which occurs in numerical simulations of an open pit excavation. Hence, the impact of coefficient α_G on the deformation is investigated for the isotropic initial stress condition ($K_0 = \sigma_h/\sigma_v = 1.0$) and homogeneous soil ground.

The geometry and mesh of the FE model are presented in Fig. 2. The mechanical behaviour of 20.0 m thick stiff clay layer ($\gamma_{\text{sat}} = 20.0$ kN/m^3) is described by the proposed anisotropic model. The initial groundwater table is located 1.0 m under the ground level. Symmetry of the BVP is taken into account and only the half of the excavation is included in the FE model. The excavation is simulated in 4 phases of soil removal and dewatering performed as a coupled deformation-flow analysis. The applied value of permeability coefficient $k_v = k_h = 1 \cdot 10^{-4}$ m/day and the time scheduled for all excavation phases (10 days) practically correspond to the undrained conditions. Closed flow boundaries are applied on the symmetry and bottom boundaries whereas constant water head (–1.0 m) is applied on the right boundary. Seepage conditions are assumed on the top of the model as well as on the sides and bottom of the excavation. The following values of the model material parameters are used:

- Small strain stiffness:
  $G^{\text{ref}}_{0vh} = 50000$ kPa, $\beta = 0.3$, $\alpha_G = 0.7, 1.0, 3.0$, $p_{\text{ref}} = 100$ kPa;
- Strain degradation:
  $N_{\text{b}} = 10$, $G^{\text{ref}}_{vh_{t\,\text{min}}} = 0.1 \cdot G^{\text{ref}}_{0vh} = 5000$ kPa, $\|\boldsymbol{\varepsilon}\|_{\text{sh}} = 0.0007$;
- Shear strength criterion:
  $\phi = 27^\circ$, $c = 20$ kPa, $\psi = 3^\circ$, $p_{\text{te}} = 0$ kPa.

The results obtained from the FE simulations are presented in Fig. 2 and Fig. 3. The selected range of the cross-anisotropy coefficient α_G values (i.e. $\alpha_G = 0.7$ up to $\alpha_G = 3.0$ implying higher vertical and higher horizontal stiffness respectively) represents limits known from the experimental evidence for different soils [6, 14]. However, in stiff

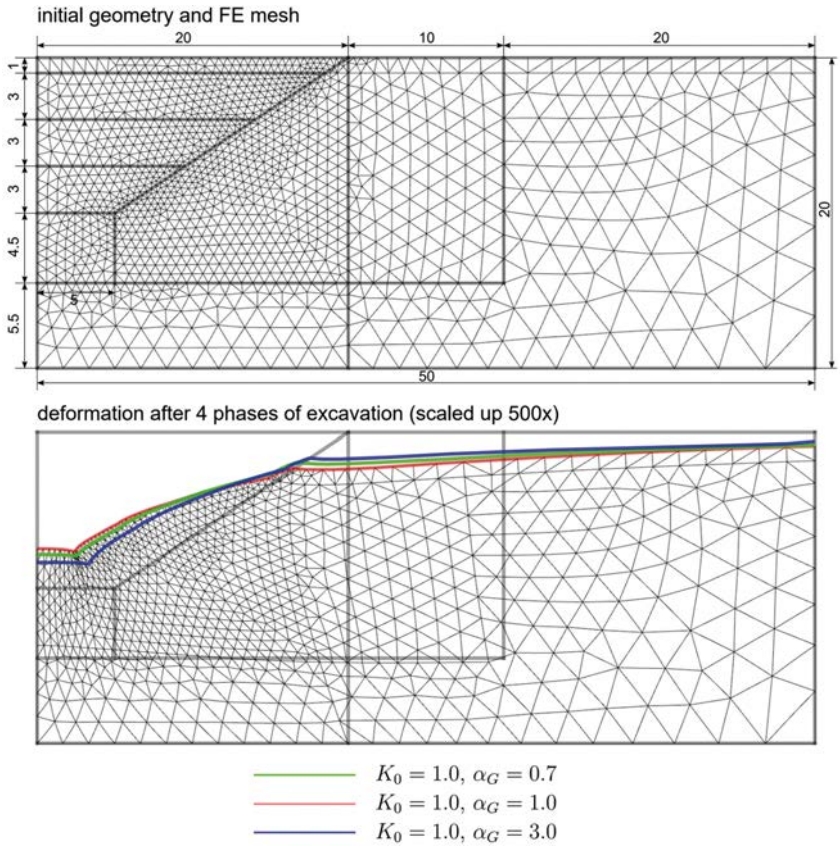

Fig. 2. Plane strain FE model of the exemplary excavation problem in homogeneous soil and comparison of deformed ground profiles calculated after excavation simulations for different α_G values

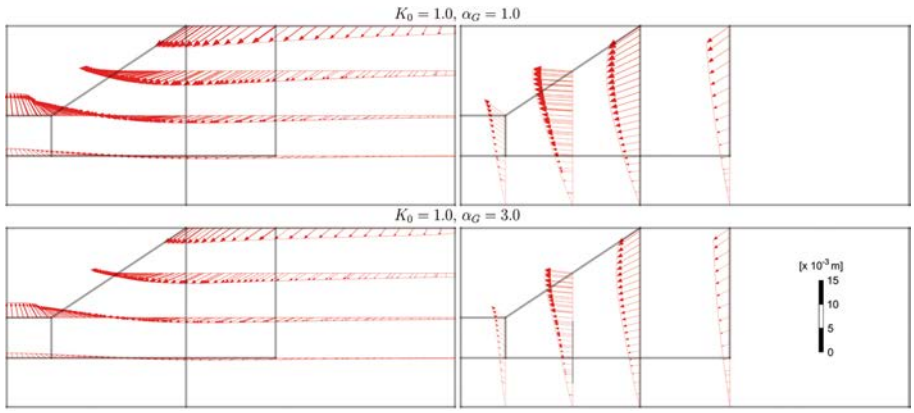

Fig. 3. The exemplary excavation problem – comparison of displacement profiles in horizontal and vertical sections calculated for the isotropic case and high degree of inherent cross-anisotropy ($\alpha_G = 3.0$)

overconsolidated clays a higher horizontal stiffness prevails. Comparison of the ground profiles after excavation for all examined values of α_G and the background of the deformed mesh obtained for the reference initially isotropic case ($K_0 = 1.0$, $\alpha_G = 1.0$) is presented in Fig. 2. The settlement of the ground surface, heave of the excavation bottom and horizontal displacement of the excavation slope are the highest for the isotropic case ($\alpha_G = 1.0$). The deformed ground profiles for $\alpha_G = 0.7$ and $\alpha_G = 1.0$ do not differ significantly from each another. Therefore, for clarity, continuous displacement profiles in the selected horizontal and vertical profiles are compared in Fig. 3 only for $\alpha_G = 1.0$ and high horizontal stiffness ($\alpha_G = 3.0$). In both cases the stress evolves from the initial isotropic state to an anisotropic one after the excavation with high stress obliquities and rotations of the principal components. At the end of excavation the stress distributions are similar excluding the area closest to the bottom of the excavation. This is the area where differences between displacement fields are the highest. However, the differences in displacements are quite small quantitatively regarding the applied ultimate values of α_G.

4. Back analysis of the trial open pit excavation

The back analysed case study concerns the real scale trial open pit excavation in Oxford Clay at Elstow site, Hertfordshire, UK. The detailed description of the research as well as the extensive laboratory testing of Oxford Clay properties is presented in PhD thesis by Pierpoint [4]. The dimensions of the construction at the surface level were 38 ×104 m with depth of 10 meters. The appropriate measuring instrumentation was installed to survey the excavation induced deformations. The full geometry of a pit along with the schematics of instrumentation location and soil profile is shown in Fig. 5 and Fig. 7. The excavation was symmetric and only its half is shown in figures, however, the displacement measurement points were located on both sides of the symmetry line. The details of measurement techniques are given in [4, 5] and the presented displacements at the measurement points located in one cross-section are averaged from different devices located close to each other. The groundwater level was 1.0 m below the ground level. The excavation was conducted in four phases that took 10, 2, 5 and 26 days respectively. Displacements in the measurement points are reported after two consolidation phases – 6 days and 84 days after finishing the excavation.

The values of material parameters of the soil layers are adopted from [4,5]. The bottom Kellaways layers are generally very stiff and the most important parameters influencing the deformation are stiffness parameters of the Oxford Clay. Hence, during calibration of the hyperelastic-plastic model parameters in the element tests also more recent experimental evidence is taken into account [25]. Exemplary calibrations in element test are shown in Fig. 4.

Parameters of all soil layers simulated with the anisotropic hyperelastic-plastic model are listed in Table 1. The top layer of clayey head deposits is simulated with the Mohr-Coulomb model ($\gamma = 18$ kN/m^3, $\phi = 30°$, $c = 10$ kPa, $\psi = 0°$, $E_{oed} = 60000$ kPa, $\nu = 0.3$, $k_v = k_h = 0.01$ m/day, $K_0 = 1.0$).

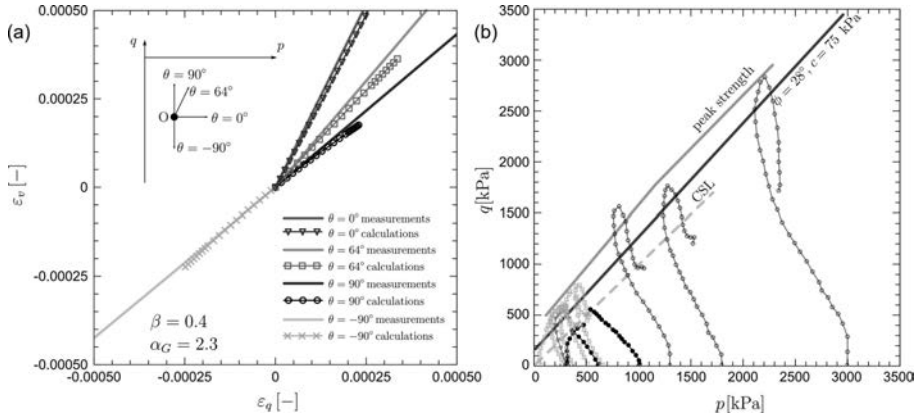

Fig. 4. Calibration of model parameters for Oxford Clay with available triaxial test results: (a) proportional drained stress paths [5], (b) CIU tests [25]

Table 1. Parameters of the geotechnical layers simulated with the hyperelastic-plastic model

	Parameter	Weathered Oxford Clay	Oxford Clay	Kellaways Clay	Kellaways Sand
Small strain stiffness	G^{ref}_{0vh}	120000 kPa	120000 kPa	157300 kPa	157300 kPa
	β	0.4	0.4	0.5	0.5
	α_G	2.3	2.3	1.7	1.7
	p_{ref}	100 kPa	100 kPa	100 kPa	100 kPa
Strain degradation	$G^{\text{ref}}_{vh_{t\,\min}}$	7000 kPa	10000 kPa	10000 kPa	10000 kPa
	$\|\boldsymbol{\varepsilon}\|_{\text{sh}}$	$0.5 \cdot 10^{-3}$	$0.5 \cdot 10^{-3}$	$1.0 \cdot 10^{-3}$	$1.0 \cdot 10^{-3}$
Shear strength criterion	ϕ	28°	28°	30°	30°
	c	50 kPa	75 kPa	30 kPa	20 kPa
	ψ	3°	3°	3°	3°
	p_{te}	1 kPa	1 kPa	1 kPa	1 kPa
Flow	$k_v = k_h$	$0.0518 \cdot 10^{-3}$ m/day	$0.0518 \cdot 10^{-3}$ m/day	$0.0518 \cdot 10^{-3}$ m/day	$3.46 \cdot 10^{-3}$ m/day
Unit weight & initial stress	γ	18.5 kN/m^3	17.5 kN/m^3	19.5 kN/m^3	19.5 kN/m^3
	K_0	1.8	1.8	1.5	1.5

4.1. Plane strain model

The geometry and mesh of the plane strain model are presented in Fig. 5. Location of the analysed cross-section is shown in Fig. 7. The FE modelling procedure of the open pit excavation is analogous to that presented in Section 3. Additionally, after the excavation two consolidation phases are executed. The results of the numerical simulations are compared with available displacement measurements in Fig. 6. It should be noted that the measured

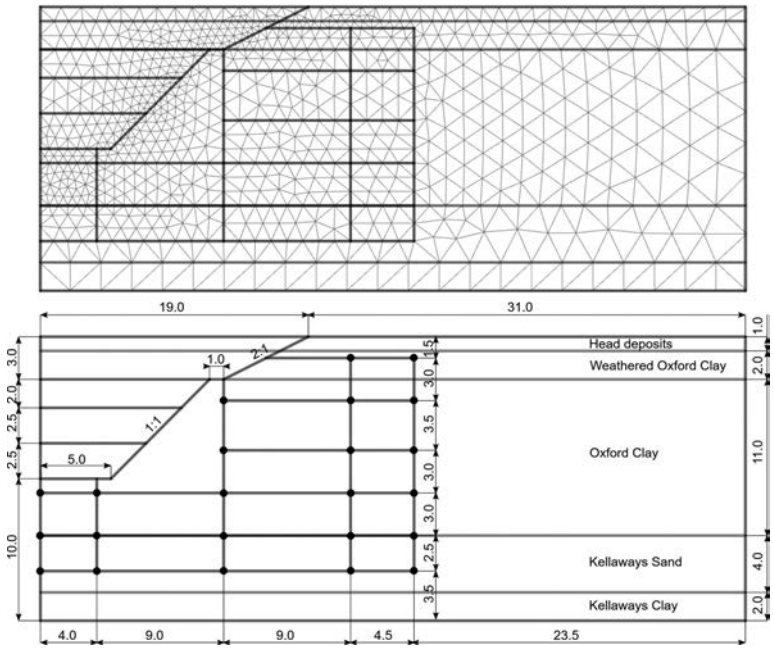

Fig. 5. Geometry, geotechnical layers, mesh of the plane strain model and displacement measurement points of the open pit trial excavation in Oxford Clay at Elstow site

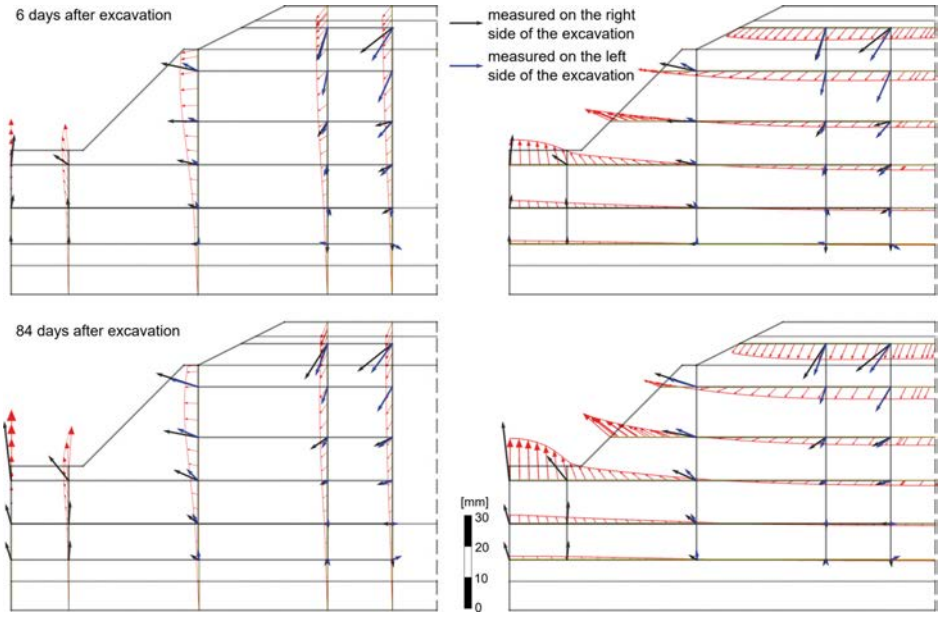

Fig. 6. Plane strain model, calculated displacement profiles and measurements

displacements on both sides of the excavation are not symmetric, unlike assumed in the geological survey and consequently in the modelling. It indicates natural differences in soil stratification or drainage conditions. The calculated displacements and measurements are most consistent in the area of excavation bottom. On the banks of excavation the calculated displacements are closer to the measurements on the left side of the excavation. The largest differences between the calculated and measured displacements occur in the area located furthest from the symmetry axis.

4.2. 3D model

The geometry and mesh of the 3D model are presented in Fig. 7. In the 3D version of the applied FE code the vertical axis is $\mathbf{v} = [0, 0, 1]^T$, which leads to anisotropic microstructure tensor $\mathbf{M} = \mathrm{diag}(0, 0, 1)$, according to Eq. (2.2). The FE modelling sequences of the open

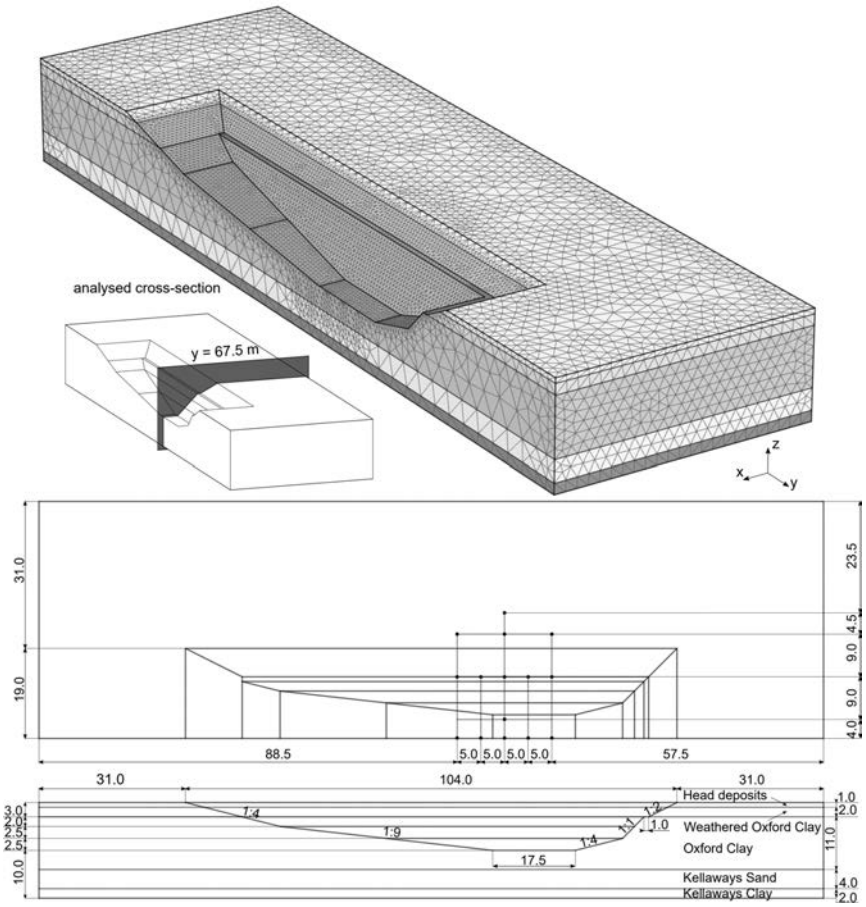

Fig. 7. Geometry and mesh of the 3D FE model of the open pit trial excavation

pit excavation are the same as in the case of the plane strain model. In the subsequent calculation phases volumes related to the layers in the plane strain model are deactivated in the scheduled time. The results of the numerical simulations are compared with the available displacement measurements in Fig. 8. The comparison is presented in the cross-section at y = 67.5 m (Fig. 7) that corresponds to the plane strain model. When compared to the alternative cross-sections that can be obtained from the 3D model results, this one has the largest displacements. The calculated displacements agree better with the measurements than in the case of the plane strain model in the area close to the excavation (e.g. displacement profile in horizontal cross-section positioned 1.0 m under the excavation bottom). However, the calculated displacements are still too small and even smaller to those calculated in the plane strain model in the cross-sections located furthest from the symmetry axis. Generally, the deformation obtained from the calculations both in the plane strain and 3D models are closer to the measurements on the left side of the excavation.

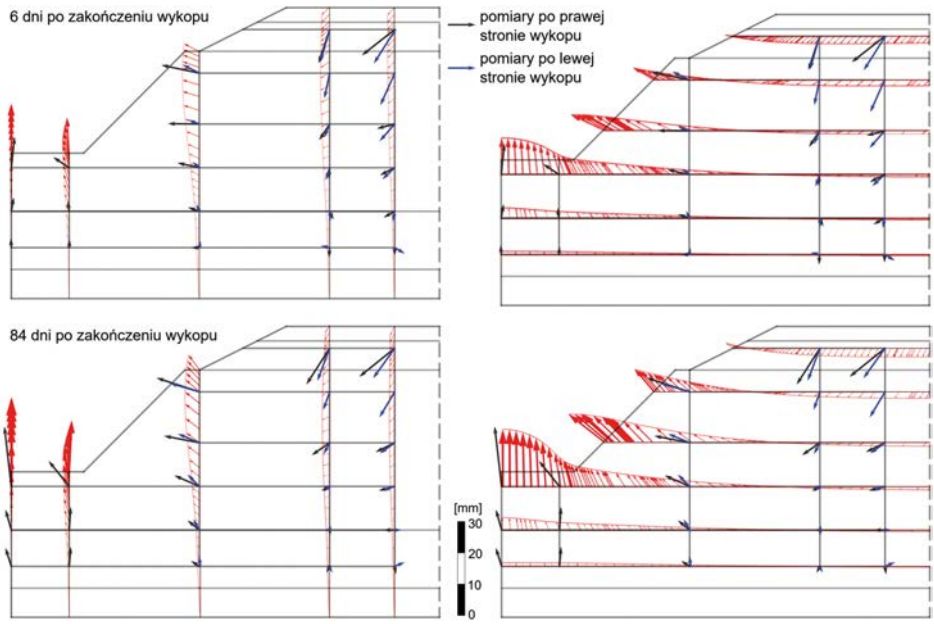

Fig. 8. 3D model, calculated displacement profiles and measurements

5. Conclusions

The article's primary objective was to assess the applicability of the developed anisotropic hyperelastic-plastic model in the FE analyses of the real scale geotechnical case study. The model is intended primarily for simulations of the mechanical behaviour of stiff overconsolidated soils in the pre-failure range. The main constitutive assumption was to describe the anisotropic characteristic only in the small strain hyperelastic kernel of the

model and to propagate the anisotropy for intermediate strains up to the failure by the stiffness degradation procedure. This method allows to limit the number of parameters and to use mainly standard material constants.

The case study analysed in the article is taken from the literature and concerns the extensive experimental investigation of the trial open pit excavation in highly anisotropic Oxford Clay at Elstow, UK. The results of both high quality laboratory tests of Oxford Clay and field measurements during the trial excavation are available serving as the ideal basis to perform the back analysis where the developed constitutive model may be applied, calibrated and verified.

The outcomes of the back analysis are satisfactory, particularly in the area closest the excavation. The magnitudes and directions of the calculated displacements are sufficiently accurate. Sources of unavoidable discrepancy between the calculated and measured displacements should be attributed not only to the material model but also to the limited accuracy of geological survey, seepage properties and ground water boundary conditions in the coupled deformation-flow analysis.

References

[1] T.I. Addenbrooke, D.M. Potts, and A.M. Puzrin, "The influence of pre-failure soil stiffness on the numerical analysis of tunnel construction", *Géotechnique*, vol. 47, no. 3, pp. 693–712, 1997, doi: 10.1680/geot.1997.47.3.693.

[2] C.W.W. Ng, E.H.Y. Leung, and C.K. Lau, "Inherent anisotropic stiffness of weathered geomaterial and its influence on ground deformations around deep excavations", *Canadian Geotechnical Journal*, vol. 41, no. 1, pp. 12–24, 2004, doi: 10.1139/t03-066.

[3] A. Brosse, R. Hosseini Kamal, R.J. Jardine, and M.R. Coop, "The shear stiffness characteristics of four Eocene-to-Jurassic UK stiff clays", *Géotechnique*, vol. 67, no. 3, pp. 242–259, 2017, doi: 10.1680/jgeot.15.P.236.

[4] N.D. Pierpoint, "The prediction and back analysis of excavation behaviour in Oxford Clay", PhD thesis, The University of Sheffield, United Kingdom 1996.

[5] C.C. Hird and N.D. Pierpoint, "Stiffness determination and deformation analysis for a trial excavation in Oxford Clay", *Géotechnique*, vol. 47, no. 3, pp. 665–691, 1997, doi: 10.1680/geot.1997.47.3.665.

[6] M. Cudny, *Some aspects of the constitutive modelling of natural fine grained soils*. Gdansk: Faculty of Civil and Environmental Engineering, Gdańsk University of Technology, Wydawnictwo IMOGEOR, 2013.

[7] M. Cudny and K. Staszewska, "A hyperelastic model for soils with stress-induced and inherent anisotropy", *Acta Geotechnica,* vol. 16, no. 7, pp. 1983–2001, 2021, doi: 10.1007/s11440-021-01159-z.

[8] M. Cudny and E. Partyka, "Influence of anisotropic stiffness in numerical analyses of tunnelling and excavation problems in stiff soils", in *Proceedings of the 19th International Conference on Soil Mechanics and Geotechnical Engineering*, L. Woojin. Seoul: ISSMGE, 2017, pp. 719–722.

[9] M. Cudny, K. Lisewska, M. Winkler, and T. Marcher, "Modelling tunnelling-induced deformation in stiff soils with a hyperelastic-plastic anisotropic model", submitted to *Acta Geotechnica*, 2023.

[10] R.B.J. Brinkgreve, S. Kumarswamy, W.M. Swolfs, L. Zampich, and N. Ragi Manoj, *Plaxis finite element code for soil and rock analyses*. Plaxis bv, Bentley Systems, Incorporated, 2022.

[11] P.A. Vermeer, "A five constant model unifying well established concepts", in *Constitutive relations of soils*. Rotterdam: Balkema, 1985, pp. 175–197.

[12] J.P. Boehler and A. Sawczuk, "On yielding of oriented solids", *Acta Mechanica*, vol. 27, pp. 185–206, 1977, doi: 10.1007/BF01180085.

[13] J. Graham and G.T. Houlsby, "Anisotropic elasticity of a natural clay", *Géotechnique*, vol. 33, no. 2, pp. 165–180, 1983, doi: 10.1680/geot.1983.33.2.165.

[14] D. Mašín and J. Rott, "Small strain stiffness anisotropy of natural sedimentary clays: review and a model", *Acta Geotechnica*, vol. 9, no. 2, pp. 299-312, 2014, doi: 10.1007/s11440-013-0271-2.

[15] D.J. Pickering, "Anisotropic elastic parameters for soil", *Géotechnique*, vol. 20, no. 3, pp. 271–276, 1970, doi: 10.1680/geot.1970.20.3.271.

[16] B. Simpson, J.H. Atkinson, and V. Jovičić, "The influence of anisotropy on calculations of ground settlements above tunnels", in *Geotechnical Aspects of Underground Construction in Soft Ground*. Rotterdam: Balkema, 1996, pp. 591–594.

[17] Z. Mróz, "On the description of anisotropic workhardening", *Journal of the Mechanics and Physics of Solids,* vol. 15, no. 3, pp. 163–175, 1967, doi: 10.1016/0022-5096(67)90030-0.

[18] A.M. Puzrin and G.T. Houlsby, "Strain-based plasticity models for soils and the BRICK model as an example of the hyperplasticity approach", *Géotechnique*, vol. 51, no. 2, pp. 169–172, 2001, doi: 10.1680/geot.2001.51.2.169.

[19] T. Länsivaara and S. Nordal, "A soil model for the overconsolidated region of clays", in *4th European Conference on Numerical Methods in Geotechnical Engineering, NUMGE98*. Udine: Springer, 1998, pp. 347–356.

[20] S.D. Clarke and C.C. Hird, "Modelling of viscous effects in natural clays", *Canadian Geotechnical Journal*, vol. 49, no. 2, pp. 129–140, 2012, doi: 10.1139/t11-084.

[21] K.C. Ellison, K. Soga, and B. Simpson, "A strain space soil model with evolving stiffness anisotropy", *Géotechnique*, vol. 62, no. 7, pp. 627–641, 2012, doi: 10.1680/geot.10.P.095.

[22] M. Cudny and A. Truty, "Refinement of the Hardening Soil model within the small strain range", *Acta Geotechnica*, vol. 15, no. 8, pp. 2031–2051, 2020, doi: 10.1007/s11440-020-00945-5.

[23] H. Matsuoka and T. Nakai, "Stress-strain relationship of soil base on the SMP, constitutive equations of soils", in *Proceedings of the 9th International Conference on Soil Mechanics and Foundation Engineering, Speciality Session*. Tokyo, 1977, pp. 153–162.

[24] B. Jeremić and S. Sture, "Implicit integrations in elastoplastic geotechnics", *Mechanics of Cohesive-frictional Materials*, vol. 2, no. 2, pp. 165–183, 1997, doi: 10.1002/(SICI)1099-1484(199704)2:2<165::AID-CFM31>3.0.CO;2-3.

[25] R. Hosseini Kamal, M.R. Coop, R.J. Jardine, and A. Brosse, "The post-yield behaviour of four Eocene-to-Jurassic UK stiff clays", *Géotechnique*, vol. 64, no. 8, pp. 620–634, 2014, doi: 10.1680/geot.13.P.043.

Wpływ anizotropii sztywności podłoża gruntowego na odkształcenie wywołane otwartym wykopem

Słowa kluczowe: anizotropia sztywności gruntów, małe odkształcenia, sztywne grunty prekonsolidowane, otwarty wykop, modelowanie MES w geotechnice

Streszczenie:

Modelowanie numeryczne zagadnień geotechnicznych związanych z odciążeniem podłoża (np. tunelowanie, wykopy) wymaga odpowiedniego opisu materiałowego gruntu, który pozwala na prawidłową symulację charakterystyki mechanicznej w zakresie małych odkształceń. Najważniejszymi elementami są tutaj nieliniowość sztywności związana z barotropią oraz degradacją stycznego modułu ścinania z odkształceniem oraz inherentna anizotropia sztywności. Modele konstytutywne dostępne w popularnych systemach obliczeniowych rzadko pozwalają na uwzględnienie anizotropii sztywności w zakresie małych odkształceń. Najczęściej przyczyną jest bardziej skomplikowana procedura implementacji niż w przypadku modeli z izotropową sztywnością, jak również ograniczona dostępność parametrów materiałowych związanych z anizotropią. Rozwój technik pomiarowych w eksperymentalnej mechanice gruntów, obserwowany w ostatnich latach na całym świecie, pozwala jednak na zaprojektowanie i przeprowadzenie badań anizotropii sztywności w warunkach ważnych inwestycji lub

projektów badawczych. Najczęściej jest to pomiar współczynnika anizotropii α_G w aparacie trójosiowym wyposażonym w elementy sejsmiczne bender zorientowane zarówno w pionie jak i w poziomie. System taki pozwala na bezpośrednie wyznaczenie modułów ścinania w płaszczyźnie pionowej G_{vh} oraz poziomej G_{hh} ($\alpha_G = G_{hh}/G_{vh}$). W artykule przedstawiono własny hipersprężysto-plastyczny model konstytutywny uwzględniający zarówno nieliniowość jak i anizotropię sztywności w zakresie małych odkształceń. W modelu tym wykorzystano anizotropową hipersprężystość do opisu sztywności początkowej, system zagnieżdżonych powierzchni plastyczności w przestrzeni odkształcenia do opisu degradacji sztywności (tzw. model Brick) oraz konwencjonalne kryterium wytrzymałości na ścinanie do ograniczenia dewiatorowych stanów naprężenia. Model zostałzaimplementowany w programie metody elementów skończonych *Plaxis* w ramach opcji User Defined Soil Model (UDSM). Analizowanym zagadnieniem brzegowo początkowym jest próbny otwarty wykop wykonany w ile oxfordzkim w Elstow, Wielka Brytania. Szeroka baza danych dotyczących niestandardowych badań laboratoryjnych iłu oksfordzkiego zorientowanych, oprócz wyznaczenia parametrów standardowych, na charakterystykę anizotropii sztywności dostępna jest w literaturze. Dokładny opis realizacji wykonanego próbnego wykopu z danymi pozwalającymi na przeprowadzenie własnych analiz wraz z wynikami monitoringu przemieszczeń dostępne są w publikacji Hird&Pierpoint (Geotechnique 47(3), 1997). Umożliwiło to, kalibrację parametrów anizotropowego modelu hipersprężysto-plastycznego i przeprowadzenie analizy wstecz będącej cenną weryfikacją przydatności opracowanego modelu konstytutywnego. Przed wykonaniem symulacji numerycznych próbnego wykopu w Elstow przeprowadzono również serię obliczeń na uproszczonym przykładowym modelu wykopu otwartego w płaskim stanie odkształcenia w celu rozpoznania wpływu czystej anizotropii inherentnej na deformację powstającą podczas odciążenia podłoża gruntowego takim wykopem. Symulację numeryczną wykopu próbnego w Elstow przeprowadzono zarówno w płaskim stanie odkształcenia jak i na modelu przestrzennym. Metoda symulacji odpowiadała podejściu sprzężonemu konsolidacji z równoczesnym uwzględnieniem przepływu wody w gruncie (*coupled deformation flow analysis*). Warunki czasowe wykonania wykopu próbnego, jak również parametry filtracyjne oraz mechaniczne zalegających gruntów powodują jednak, że przedmiotowe zagadnienie brzegowo-początkowe zachodzi ostatecznie w warunkach bliskich warunkom braku drenażu. Wyniki przeprowadzonych symulacji numerycznych porównano z wynikami monitoringu przemieszczenia. Uzyskano zadowalającą zgodność obliczonego i pomierzonego pola przemieszczenia. Dokładność wyników obliczeń jest jednak zmienna w zależności od obszaru analizowanego zagadnienia. Odpowiednie porównania przedstawiono na rysunkach w artykule.

Received: 2023-03-27, Revised: 2023-03-28